Original Article | Journal of Biosystems Engineering

J. of Biosystems Eng. 42(4):265-275. (2017. 12)
https://doi.org/10.5307/JBE.2017.42.4.265

eISSN : 2234-1862
pISSN : 1738-1266

Design and Application of Subsurface Drainage Devices for Multipurpose Farmland

Jong Gil Jeon*, Yong Hun Choi, Min Young Kim, Young Gjin Kim

National Institute of Agricultural Sciences, Rural Development Administration, Jeonju, Republic of Korea

Received: November 6th, 2017; Revised: November 16th, 2017; Accepted: November 24th, 2017

Abstract

Purpose: This study aims to identify the most stable boring shape among the circle, square, and inverted-triangle types in order to be applied to the development of a tractor-pulled underdrain boring device. **Methods:** The underdrain boring devices designed with the circle, inverted triangle, and square types were analyzed by numerical analysis, and they were evaluated by soil moisture and underground water level in the test field. **Results:** The results of the numerical analysis indicated that the increases in displacement, and strain when a uniform load is placed on the surface soil with soil weight were in the order of the inverted-triangle type, square type, and circle type. The soil moisture content and the underground water level after rainfall showed the largest difference in the order of the circle type, square type, and inverted-triangle type, indicating that the circle type had the largest drainage effects after rainfall. **Conclusions:** The overall findings of this study show that the circle type is the most stable among the circle, square, and inverted-triangle types.

Keywords: Electrical Conductivity (EC), Numerical analysis, Soil moisture, Subsurface drain device, Underground water level

Introduction

In recent years, changes to the agricultural environment have resulted in the overproduction of rice as well as an increase in the farmland income by 2-10 times for upland crops as opposed to rice. Consideration has therefore been given to using new or existing reclaimed lands as farmlands (Kim et al., 2015). As the portion of upland crops in rice paddies has increased consistently from 7.7% in 1990, 8.2% in 2000, 9.9% in 2010, and 13% in 2012, the need for a technological response has also increased (Kim et al., 2017). The government has also sought to intervene to prevent the oversupply of rice and to stabilize the farming industry by leading the thrust to decrease rice prices to a reasonable level, as well as by introducing rice-production control policies by 2018. These policies are aimed at providing the differences in income to be derived from planting other crops instead of rice in rice paddies. This support is in the form of grants, with the goal of reducing the cultivated area of rice by 100,000 ha. over two years, followed by 50,000 ha. in 2018, and 50,000 ha. in 2019; this would represent 1/8th of the total area for rice cultivation.

To cultivate upland crops in rice paddy fields, it is important to remove the excessive moisture in the ground by improving drainage; the method primarily used to remove moisture quickly is called underdraining. Doh et al. (1994) installed underdrainage plots in rice paddies with poor drainage, speeding up the underground drainage process. They then examined the physical properties of the soil. By comparing the surface drainage plot to the control plots, the results indicated that the underdrainage plots showed improvements in permeability, water resistance aggregate, pitching strength, frictional resistance, and shearing resistance, as well as reductions in soil moisture content, bulk density and soil hardness, transitioning into soil that is appropriate for cropland.

***Corresponding author:** Jong Gil Jeon
Tel: +82-63-238-4155; **Fax:** +82-63-238-4145
E-mail: jjkfoc@korea.kr

The purpose of underdrainage in a poorly drained farmland is to remove the excessive moisture around the root and to improve the permeability of the soil, hence stopping the process of soil reduction due to a lack of soil-oxygen content and minimizing moisture stress. Ultimately, this is expected to increase the crop productivity and improve the growth environment (Skaggs et al. 1982). Ji (1981) set the surface drainage for upland crops in rice paddies to 50 mm/day as a target, the allowable days of surface water retention of one day, the ground-water level after 2-3 days post rainfall as 40-50 cm, and the coefficient of permeability as 10^{-4} cm/s; this study reported that the ground-water level from the infiltration water needed to be restrained, and the ground-water level should be contained at a depth 0.5-0.6 m underneath the surface.

Although rice paddies could be used as cropland, it is important to be able to switch back to rice paddies during periods of food shortages. As such, there is a need for technology to dynamically enable a shift between paddies and cropland to expand the production of upland crops, and to solve drainage issues and enable rapid recovery at a low cost. For non-material underdrain, which makes paddy-upland rotation easier, the mole drainage causes the underdrain phenomenon to be destroyed with time from the actual boring, and the underdrain eventually fails to perform its functions. This study examines the basic development of a boring device that can be towed by tractors and used for underdrains, and the study focuses on the circle, inverted-triangle, and square shape types using numerical analysis. Further, it focused on boring the paddy soil using the non-material underdrain method in the test field, and evaluating the changes in soil moisture and the ground-water level to identify the most stable boring shape.

Materials and Methods

Test field

The test field was located in the reclaimed land test field of the National Institute of Crop Science, located in Gyehwa-ri, Gyehwa-myeon, Buan-gun, Jeollabuk-do Province, South Korea. The test field was formed in 2010, and seven years had elapsed since its conversion to a rice paddy; while there were issues with soil-salinity concentration in the early days of its conversion, it had since recovered sufficiently to allow for crop production. As shown in Figure 1, the experiment involved the use of an underdrain boring test plots according to each shapes (1,920 m^2) and the test plots according to the distance from the boring hole (1,920 m^2). Using an underdrain boring shape, the test plots were divided into the categories: circle-type, inverted-triangle type, and square-

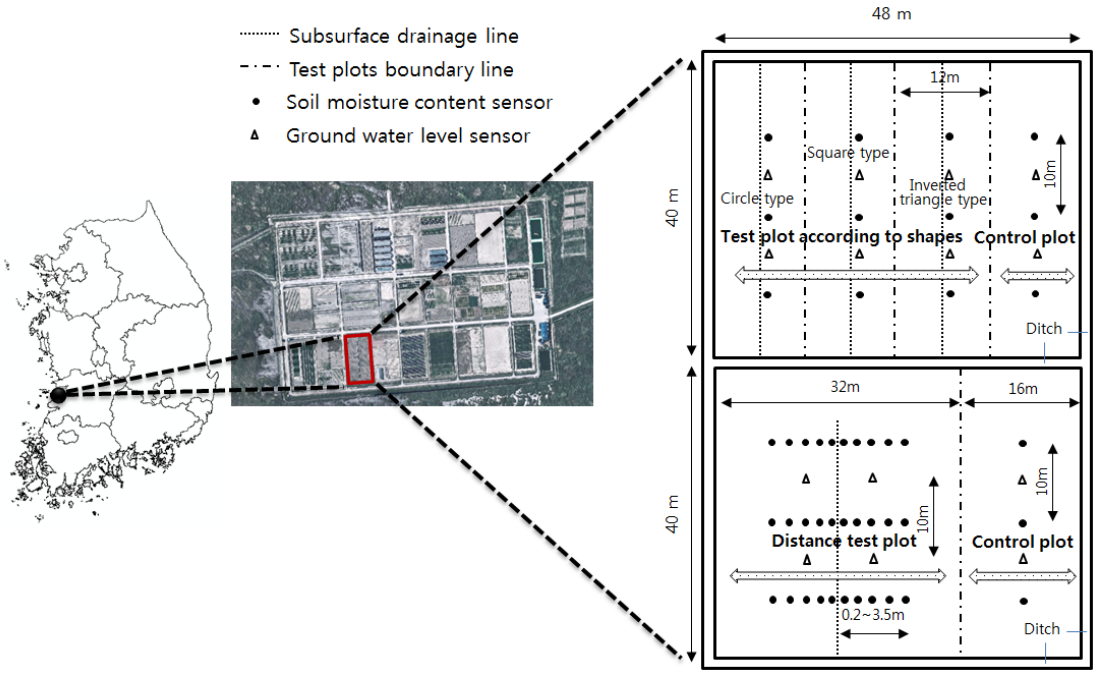

Figure 1. Geographical description of study area and location of measuring points.

type treatment plot, and control plot; the size of the treatment plots were each 12 m wide and 40 m long. The test plots, according to the horizontal distance from the boring hole, were divided into the treatment plot (1,280 m^2, 32 × 40 m) and the control plot (640 m^2, 16 × 40 m).

The analysis of the soil physical properties was performed using sieve analysis aggregates (KS F 2502) and the test for permeability (KS F 2302) to analyze the texture of the soil, the percentages of sand, loam, and clay were used to confirm the soil textural class using the soil texture triangle (USDA). The coefficient of permeability was calculated using the falling head test of the permeability test of soil (KS F 2322), and the porosity was determined by assuming the portion of soil in the total volume of the collected soil specimen (100%) as 2.65 and subtracting the portion of inorganic/organic matter.

Table 1. Physical properties of soils used in the experiment

Division/Depth	10 cm	20 cm	30 cm
Textural Class	Sandy clay loam		Sandy clay
Coefficient of permeability (cm/day)	6.64	3.23	1.75
Porosity (%)	48.30	43.90	42.40

As shown in Table 1, the textural class of the soil 20 cm below the surface soil was found to be sandy clay loam, and the one of the soil 30 cm below the surface soil was sandy clay. The coefficient of permeability decreased from 6.64 cm/day to 1.75 cm/day depending on the depth, while the porosity, including liquid and gaseous, dropped from 48.3% to 42.4%.

Design and manufacture of underdrain boring device

To underdrain boring shapes: the circle type, inverted-triangle type, and square type were compared in terms of their effectiveness (Table 2). The standard measurements for the boring device supports were set to be equivalent to the support for the tractor subsoiling blades, ensuring compatibility with the towing devices of existing tractors. In designing the shape of the boring part, for the circle type, previous research (Chung, 1995; Lee et al., 2006)

Table 2. Design and manufacture of subsurface drain devices

Type	Circle type	Inverted-triangle type	Square type
Design	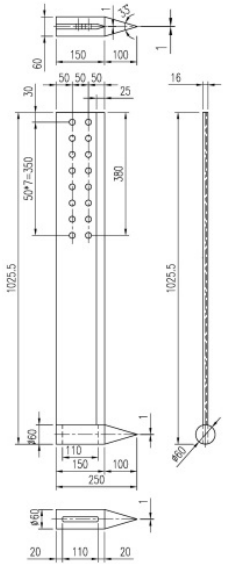	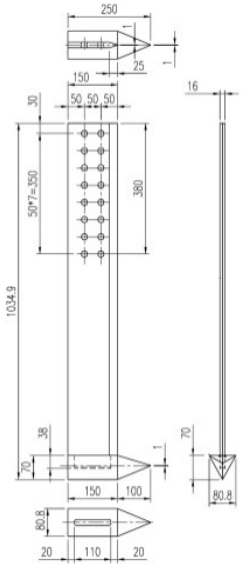	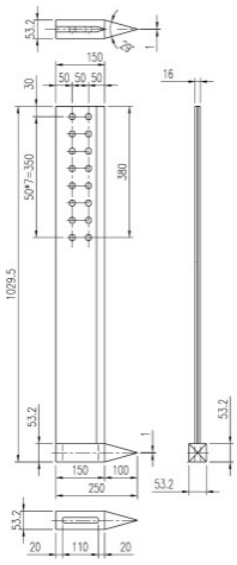
Device			

had focused on bores with sizes ø45 mm, ø50 mm, and ø100 mm suction tubes; however, according to business and farm owners, the larger bores of the suction pipes will lead to an increased pull resistance for the tractor and the collapse of the bore holes, while the smaller bores will lead to blockades from soil precipitates. In this study, the diameter of the bore was set to ø60 mm, with an area of 2,826 mm^2 for the circle type. To ensure a similar area, the inverted-triangle type had an upper side length of 80.8 mm, height of 70 mm, and bore area of 2,828 mm^2; the square type had horizontal and vertical sides of 53.2 mm, and a bore area of 2,830 mm^2.

Measurement methods

The rainfall data utilized were obtained from the weather stations (http://weather.rda.go.kr/) installed on the reclaimed land belonging to the National Institute of Crop Science, which was approximately 4 km from the test field. The soil moisture and the electrical conductivity (EC) were measured using a soil moisture sensor, WT1000B (Mirae Sensor, Korea), which enables the real-time measurements of soil moisture and EC, and is a frequency-domain reflectometry (FDR) technique that evaluates the changes in soil permittivity using frequency.

If the measurement points of the soil moisture were too far away from the boring points in the underdrain shape-specific test fields, this study showed that the sensitivity to changes in soil moisture due to rainfall would drop; if it is too close, the soil would collapse at the boring spots. As such, the points were located 20 cm in a horizontal direction from the underdrain boring spots of each of the circle type, inverted-triangle type, and square type underdrain boring points and at a depth of 20 cm from the soil surface. The temporal changes to the soil moisture caused by each underdrain boring shape were assessed using the 67-hour period on July 8, 2017, which saw an accumulated rainfall of 42 mm, and showed improvements to the soil moisture.

In this study, the soil moisture content was measured at 0.2 m, 0.75 m, 1.5 m, 2.5 m, and 3.5 m away from the boring points, 20 cm underneath the surface soil, and the values obtained were compared with the control plot by examining the variations with distance. The horizontal distance test plots used the circle type as the main boring shape, and the analysis was conducted 72 hours after a 42 mm rainfall that occurred on July 8, 2017. This study showed that there would not be any significant changes for 1-2 days after the rainfall ended; as such, 72 hours were allotted for the water to drain through the underdrain.

The salt decontamination effects from the underdrain boring were analyzed using changes in the EC. In the underdrain boring test plots, the average monthly EC of the treatment plots and control plot were calculated regardless of the shape. Variations in the EC with distance for each test plot were measured 0.2 m, 0.75 m, 1.5 m, 2.5 m, and 3.5 m away from the boring points, 20 cm underneath the soil surface, and 72 hours after the 42-mm rainfall event that occurred on July 8, 2017. This is similar to the measurement method of the soil moisture content.

To measure the underground water level, the underground water level monitoring well was created by digging a hole 60 cm underneath the soil surface at a horizontal distance of 20 cm from the underdrain boring spot (digging diameter: 100 mm) using a spiral excavator, marked with △ in Figure 1. In addition, a 100 mm diameter plastic pipe was installed at the 60 cm depth. Subsequently, an ultrasonic distance sensor (UM18, Germany) was installed 7 cm upward the soil surface to measure the underground water level within the pipe of the monitoring well. The underground water level measurements of the shape-specific treatment plots were obtained by taking the three-day measurements from the 47.5 mm rainfall event on September 11, 2017, and comparing it to the control plot.

After the 43, 69, and 85 days marks, portions of the underdrain boring spots were cut, and the cross sections were compared to evaluate the durability of each boring shapes.

Numerical method analysis

Abaqus (version 4.13) was used as the program tool for numerical analysis to provide three dimensional (3D) analysis. The soil conditions used in the analysis were modulus of elasticity (E) of 245.6 kPa, Poisson's ration (γ) of 0.2, humid soil unit weight (Wh) of 18.11 kN/m^3, dried soil unit weight (Wd) of 15.47 kN/m^3, moisture ratio of 16.7%, soil cohesiveness of 5.7 kPa, angle of soil internal friction of 29.2°, and coefficient of permeability of 6.84×10^{-4} cm/s. The model standard size was set to 10 m width, 10 m length, and 1 m height for the numerical analysis. The boring location was set at 500 mm under the top surface, displaying the axis shape of the underdrain boring device.

The numerical analysis involved the Mohr-Coulomb

theory, which is often used in the prediction of the destruction of materials such as soil or snow, where the component particles are stuck together. The Mohr-Coulomb theory states that destruction occurs when the shear stress reaches the shear strength for a line within an object; the shear stress is a function of the normal stress. The Mohr-Coulomb theory is shown in Equation (1) below, where τ_f is the shear strength, c is the cohesiveness, and ϕ is the angle of internal friction.

$$\tau_f = c + \sigma \tan\phi \quad (1)$$

Figure 2 shows the Mohr circle and the Mohr failure envelope; the relationship between the maximum principal stress and the minimal principal stress is shown in Equation (2).

$$\sin\phi = \frac{OX}{DO} = \frac{OX}{DB+BO} = \frac{(\sigma_1-\sigma_3)/2}{c\cot\phi+(\sigma_1+\sigma_3)/2}$$
$$\rightarrow \sigma_1 = \sigma_3 \tan^2\left(45+\frac{\phi}{2}\right)+2c\tan\left(45+\frac{\phi}{2}\right) \quad (2)$$

Results and Discussion

Results of numerical analysis according to the bore shape

Based on the numerical analysis, at the 500 mm boring depth, the maximum stress on the self-weight of the soil in the Z-axis according to the shapes of the boring was the highest for the inverted-triangle shape at 7.70 kPa, and the lowest for the square shape at 0.01 kPa. When a uniform load of 0.01 kPa, 0.02 kPa, and 0.03 kPa were applied on the soil surface with the self-weight of the soil in the Z-axis according to shapes of the boring, the changes in stress were as follows: an increase of 4.57 kPa to the maximum value of 30.52 kPa for the circular shape; 7.70 kPa to the maximum value of 69.50 kPa for the inverted-triangle shape; and 0.01 kPa to the maximum value of 0.05 kPa for the square shape. Figure 4 indicates the stress distribution chart against the self-weight of the soil in the Z-axis according to the shapes of the boring.

The inverted-triangle shape had the largest displacement

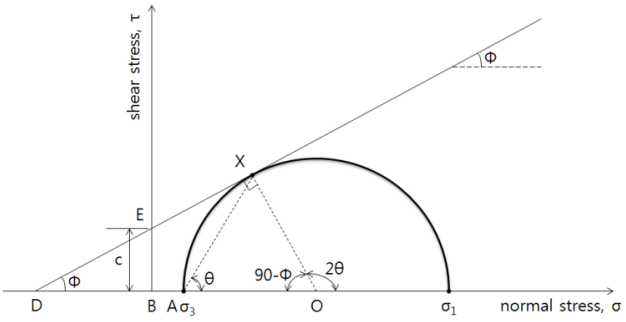

Figure 2. Mohr's failure envelope.

Table 3. Results of stress by shapes of boring according to loading condition (unit: kPa)

Shapes of boring	Soil weight	Soil weight +0.01 kPa	Soil weight +0.02 kPa	Soil weight +0.03 kPa
Circle	4.57	18.57	30.52	30.52
Inverted Triangle	7.70	20.42	41.96	69.50
Square	0.01	0.03	0.04	0.05

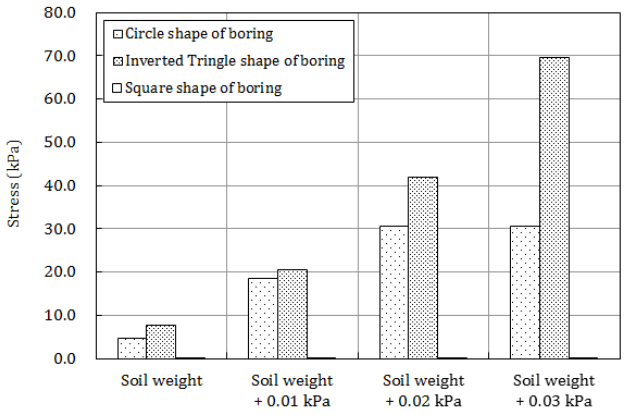

Figure 3. Stress results by shapes of boring according to loading condition.

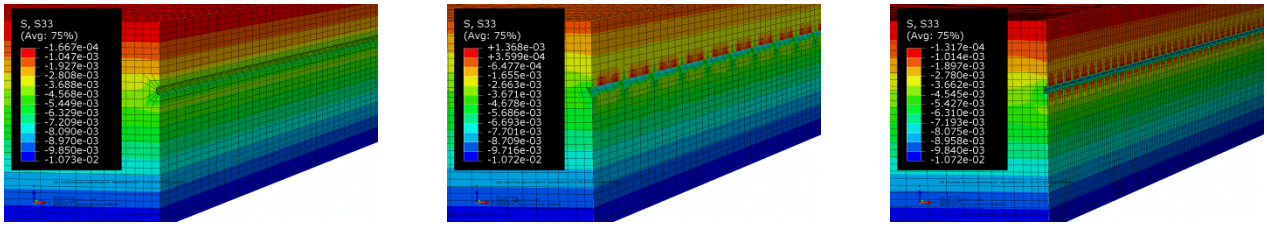

Circle shape of boring | Inverted-triangle shape of boring | Square shape of boring

Figure 4. Stress distribution chart against the self-weight of the soil in the Z-axis according to shapes of boring.

at 2.645 mm, and the circle shape had the smallest displacement at 0.124 mm on the self-weight of the soil in the Z-axis. When uniform loads of 0.01 kPa, 0.02 kPa, and 0.03 kPa were applied on the soil surface with the self-weight of the soil in the Z-axis according to shapes, the displacements were as follows: an increase of 0.124 mm to the maximum value of 72.140 mm for the circular shape; 2.645 mm to the maximum value of 315.7 mm for the inverted-triangular shape; and 1.736 mm to the maximum value of 122.9 mm for the square shape. Figure 7 indicates the displacement distribution chart by the self-weight of the soil in the Z-axis according to the shapes of the boring.

The square shape had the largest strain on the self-weight of the soil in the Z-axis at 0.028%, and the circle shape had the lowest strain at 0.007%. When uniform loads of 0.01 kPa, 0.02 kPa, and 0.03 kPa were applied on the soil surface with the self-weight of the soil in the Z-axis according to the shapes of the boring, the change in the strains were as follows: an increase of 0.007% to the maximum value of 0.098% for the circular shape; an increase of 0.017% to the maximum value of 0.896% for the inverted-triangular shape; and an increase of 0.028% to the maximum value of 0.283% for the square shape. Figure 8 indicates the strain distribution chart by the self-weight of the soil in the Z-axis according to the

Table 4. Results of displacement by shapes of boring according to loading condition (unit: mm)

Shapes of boring	Soil weight	Soil weight +0.01 kPa	Soil weight +0.02 kPa	Soil weight +0.03 kPa
Circle	0.124	36.070	81.160	72.140
Inverted Triangle	2.645	45.730	93.620	315.700
Square	1.736	40.950	90.880	122.900

Table 5. Results of strain by shapes of boring according to loading condition (unit: %)

Shapes of boring	Soil weight	Soil weight +0.01 kPa	Soil weight +0.02 kPa	Soil weight +0.03 kPa
Circle	0.007	0.053	0.098	0.098
Inverted Triangle	0.017	0.076	0.229	0.896
Square	0.028	0.092	0.147	0.283

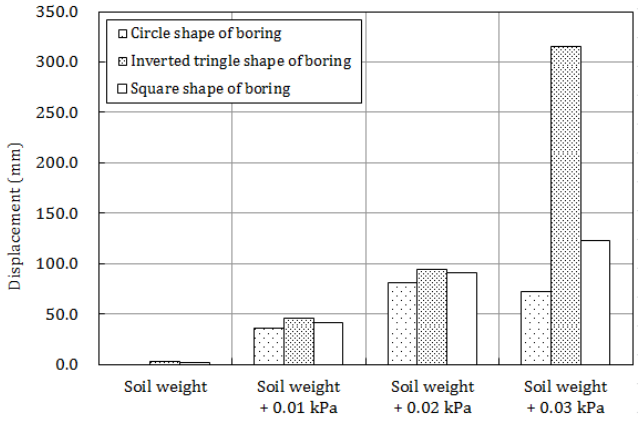

Figure 5. Displacement results by shapes of boring according to loading condition.

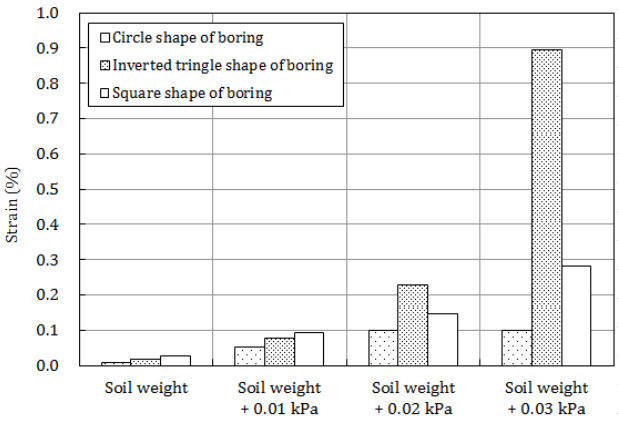

Figure 6. Strain results by shapes of boring according to loading condition.

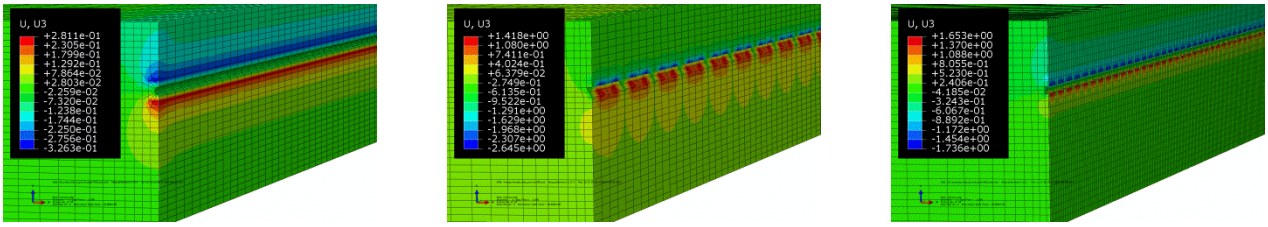

Circle shape of boring | Inverted-triangle shape of boring | Square shape of boring

Figure 7. Displacement distribution chart against the self-weight of the soil in the Z-axis according to shapes of boring.

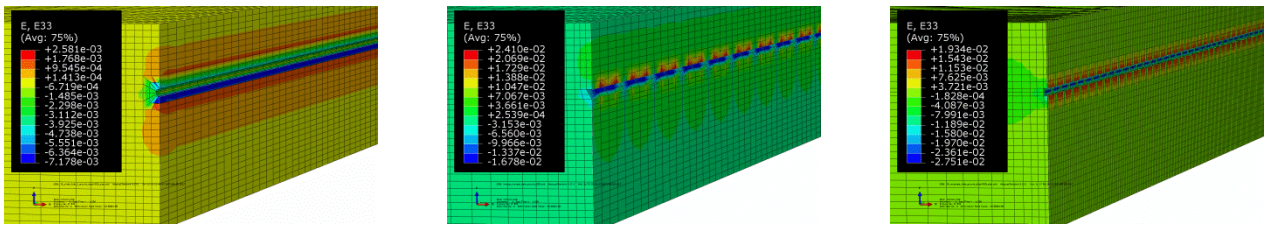

Figure 8. Strain distribution chart against the self-weight of the soil in the Z-axis according to the shapes of boring.

shapes of the boring.

The increase in displacement, and strain resulting from the application of uniform loads on the soil surface with the self-weight of the soil in the Z-axis according to the shapes of the boring were in the order of inverted-triangle, square, and circle shape.

A comprehensive evaluation of Tables 3-5 and Figures 3-8 suggest that the hole shapes of the underdrain boring would be destroyed in the order of inverted triangle, square type, and circle type when the underdrain is built on non-material underdrains such as the mole underdrain on croplands.

Variation in soil moisture according to test plot

As shown in Figure 9, between 1-6 hours after rainfall, the soil moisture is subject to rapid changes, reaching a maximum level; it decreases slowly approximately three hours after the rainfall stopped.

For the 42 mm rainfall event, the changes in the soil moisture content over 67 hours according to the treatment plots were in the order of the circle type treatment plot (47.2%), the square type treatment plot (43.3%), and the inverted-triangle type treatment plot (35.5%), and the control plot (17.5%), according to Table 6. As such, the circle type, inverted-triangle type, and square type treatment plots were different in terms of soil moisture content, with significant differences from the control plot.

The results of standard deviation and coefficient of variation of the soil moisture content according to test plots after rainfall were higher in the order of circular type plot, square type plot, inverted-triangle type plot and control plot.

In the case of the 42 mm rainfall, the soil moisture content at points 0.2, 0.75, 1.5, 2.5, and 3.5 m from the underdrain after 72 hours were 37.4, 39.6, 46.9, 61.3, and 69.7%, respectively; the soil moisture content of the control plot was rather high at 76.3%.

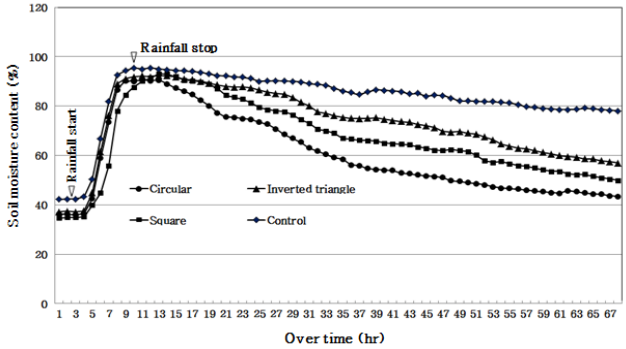

Figure 9. Variation in soil moisture content over time after 42 mm rainfall event.

Table 6. Maximum and minimum values of soil moisture content in test plots (unit: %)

Item	Circle type plot	Inverted-triangle type plot	Square type plot	Control plot
Maximum soil moisture content	90.6	92.4	93.2	95.5
Minimum soil moisture content	43.4	56.9	49.9	78.0
Average soil moisture content	61.8	75.8	69.3	86.4
Standard deviation	15.8	11.4	13.5	5.6
Coefficient of variation	25.6	15.1	19.4	6.5

As shown in Figure 10, the distance from the underdrain and the soil moisture content showed a positive correlation; the degree of changes in the soil moisture content from the underdrainage, as indicated by this study, was 69.7% at the 3.5 m mark, showing the influence of the underdrain when compared to 76.3% for the control plot. These may differ based on the soil type and the height of the ground-water level. These results agree with a study that reported that the narrower the

underdrain interval, the more the underdrain effect increases due to a larger crushed soil's area above the underdrain (Kim et al., 2003). In addition, a study reported that the underground water level between two underdrains is the highest at the midpoint, and the soil moisture content is the lowest around the underdrain (James et al., 1957).

Variation in underground water level according to treatment plots

For 72 hours after the 47.5 mm rainfall, the decrease in the underground water level was in the order of the circle type treatment plot (203 mm), the square type treatment plot (180 mm), and the inverted-triangle type treatment plot (163 mm); the control plot only saw a 49 mm decrease (Table 7). This showed a difference of 4.1, 3.7, and 3.3 times in the underground water level of the circle type, square type, and inverted-triangle type, respectively, when compared to the control plot, demonstrating the effects of the underdrain. Moreover, the shape specific treatment plots were different; this is considered to have been due to soil precipitates that accumulate within the underdrain holes after the construction of the underdrain, impacting drainage performance.

The difference between the average underground water level and the daily ground water level for the shape specific treatment plots and the control plot was 46.7 mm after 2 days, 44.7 mm after 3 days, and 41.7 mm after 1 day (Fig. 11).

The results of standard deviation and coefficient of variation of the underground water level according to test plots after the 47.5 mm rainfall increased in the order of the circular type plot, square type plot, inverted-triangle type plot and control plot (Table 7).

Variation in EC according to test plots

Tests were conducted over the four-month period from June to September, and the results were 1.26-1.82 dS/m for the control plot, and 0.94-1.32 dS/m for the circle type treatment plot, which are representative of the

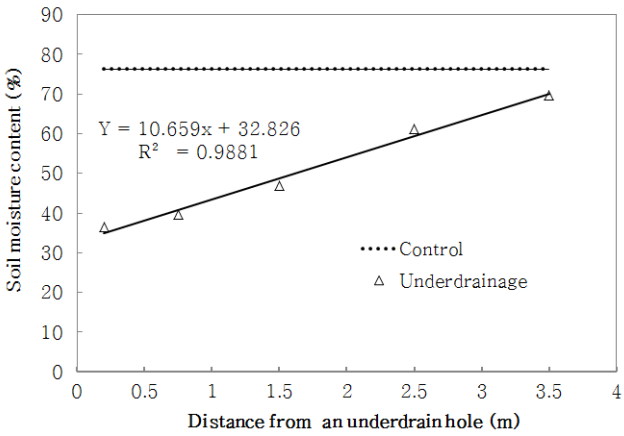

Figure 10. Relationship between soil moisture content and distance from an underdrain hole (soil depth of 20 cm).

Table 7. Variation in underground water level after 47.5 mm rainfall event

	Division	Control	Circular	Inverted triangle	Square
After 1 day	Max. level (mm)	333.0	308.0	319.0	315.0
	Min. level (mm)	317.0	244.0	267.0	258.0
	Average level (mm)	326.4	274.7	295.5	287.9
	Standard deviation (mm)	4.8	20.3	15.6	18.2
	Coefficient of variation (%)	1.5	7.4	5.3	6.3
After 2 days	Max. level (mm)	317.0	244.0	267.0	258.0
	Min. level (mm)	300.0	173.0	210.0	195.0
	Average level (mm)	308.3	209.4	239.4	228.8
	Standard deviation (mm)	5.3	21.1	18.6	19.5
	Coefficient of variation (%)	1.7	10.1	7.8	8.5
After 3 days	Max. level (mm)	300.0	173.0	210.0	195.0
	Min. level (mm)	284.0	105.0	156.0	135.0
	Average level (mm)	291.6	138.7	184.1	166.6
	Standard deviation (mm)	4.9	20.8	16.9	19.0
	Coefficient of variation (%)	1.7	15.0	9.2	11.4

shape specific treatment plots (Fig. 12). These numbers were high in June but decreased towards September. These results were similar to a study performed by Ha et al. (1997), which reported that the saline accumulations in unheated greenhouses are closely tied to the micro-meteorology within the greenhouses, leading to the highest salinity in the winter, and then decreasing generally in the order of spring, summer, and fall. As shown in this study, it appears to decrease from June to September.

This is considered to be the influence of the difference in monthly temperatures, evaporation rates, and rainfall.

The EC at horizontal distances of 0.2, 0.75, 1.5, 2.5, and 3.5 m from the underdrain are 1.21, 1.29, 1.38, 1.46, and 1.51 dS/m, respectively, with the EC at the control plot at 1.57 dS/m, indicating that the EC values were found to be smaller as it got closer the underdrain.

As shown in Figure 13, the relationship between the distance from the underdrain and EC showed a positive correlation; EC is used as an indicator of the salinity, and while the salt decontamination effect due to the under-

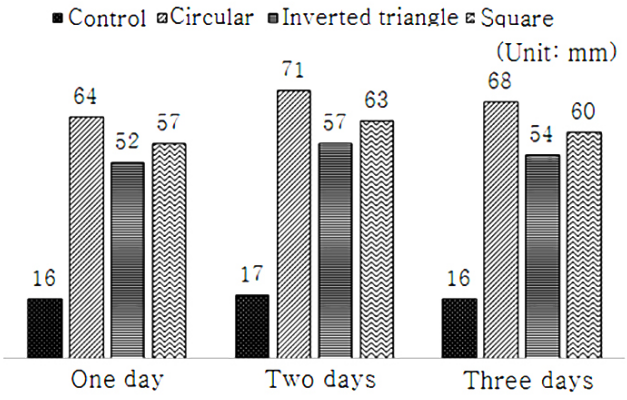

Figure 11. Daily variation in underground water level in test plots.

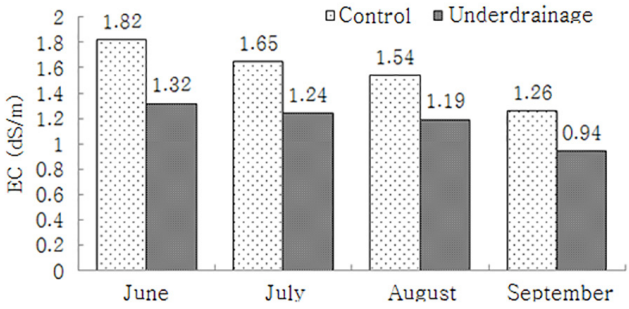

Figure 12. Monthly changes of EC for test plots at a soil depth of 20 cm.

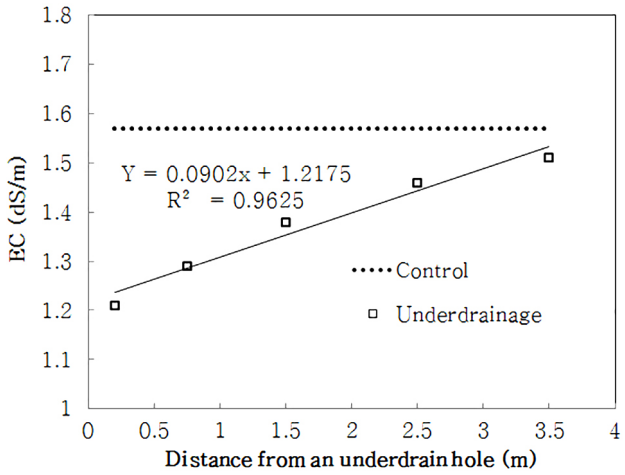

Figure 13. Relationship between soil EC and distance from an underdrain hole (soil depth of 20 cm).

Table 8. Variation in hole shapes over time

Division	After 43 days	After 69 days	After 85 days
Circle type			
Inverted-triangle shape			
Square shape			

drainage may differ based on the physical properties of soils and underground water levels, it was confirmed that the salt decontamination effect was also influenced by 3.5 m.

Variation in hole shapes over time

As shown in Table 8, an investigation into the hole shapes over time showed that a decent shape was maintained after 43 days of holing; at the 69-day mark, the hole was 1/3-1/2 blocked due to soil precipitates. At the 85-day mark, 1/2 of the hole was blocked for the circle type, 4/5 was blocked for the inverted-triangle type, and 3/4 was blocked for the square type.

Based on the results, it is estimated that the underdrainage effect will last for about three months, but it may differ according to regional weather conditions and classes of soil texture.

Conclusions

To increase the production of upland crops in rice paddies, this study focused on the development of a basic boring device that enables tractor-pulled underdrains. The boring devices are the circle type, inverted-triangle type, and square type. The shapes were analyzed using numerical analysis. Moreover, the rice paddy soils were bored using non-material underdrainage methods in the test field, and the soil moisture content, ground-water level, EC, and hole shapes were examined. The summary of the results is as follows:

(1) The results of the numerical analysis indicated that the increase in displacement, and strain when a uniform load is placed on the soil surface with soil weight were in the order of the inverted-triangle type, square type, and circle type, indicating that the inverted-triangle type was the weakest in terms of external pressure.
(2) The soil moisture content and underground water level after rainfall showed the largest difference from the investigation of underdrain shape-specific test plots in the order of the circle type, square type, and inverted- triangle type, indicating that the circle type had the largest drainage effects after rainfall.
(3) The relationship between the distance from the underdrain, soil moisture content, and the underground water level were positively correlated; the effects of soil moisture and decontamination of salt from the underdrain boring were found to be present, even at the 3.5 m mark.
(4) Eighty five days after boring, more than half of the underdrain holes were shown to be blocked due to soil precipitates; however, this may differ according to regional weather conditions and classes of soil texture.

Summarizing the numerical analysis results, and changes to soil moisture and underground water level as well as changes to hole shapes over time indicate that the circle type is the most stable among the circle, square, and inverted-triangle types. This study plans to apply these findings for the development of a tractor-pulled underdrain boring device, which is currently underway.

Conflict of Interest

The authors declare no conflict of interests.

Acknowledgement

This study was carried out with the support of "Research Program for Agricultural Science & Technology Development (Project No. PJ01201901)", National Institute of Agricultural Sciences, Rural Development Administration, Republic of Korea.

References

Chung, S. O. 1995. Analyses of subsurface drainage effects of farmland with respect to pipe and envelop material. Journal of the Korean Society of Agricultural Engineers 37(5):55 (In Korean).

Doh, D. H., S. J. Kim, S. K. Jin and R. C. Jo. 1994. A study on variation of the soil physical characteristics of multi-utilized paddy field by the introduction of subsurface drainage facility. Journal of Life Science 1:87-96.

Ha, H. S., Y. B. Lee, B. K. Sohn and U. G. Kang. 1997. Characteristics of soil electrical conductivity in plastic film house located in southern part of Korea. Journal of Soil Science and Fertilizer 30:345-350.

James, N. L. 1957. Drainage of agricultural lands. American Society of Agronomy 113-154.

Ji, G. H. 1981. Study on Subsurface drainage system for the multipurpose paddy field. Journal of the Korean Society of Agricultural Engineers 23(4):15-20.

Kim, H. T., D. U. Seo, C. H. Yoo and S. Y. Kim. 2015. Theoretical Analysis of Soil Desalination Characteristics for Underdrain System at Reclaimed Tidal Land. Journal of the Korean Society of Agricultural Engineers 57(3):87-92 (In Korean).

Kim, L. Y., H. J. Cho and K. H. Han. 2003. Effects of Tile Drain on Physicochemical Properties and Crop Productivity of Soils under Newly Constructed Plastic Film House, Korean Journal of Soil Science and Fertilizer 36(3):154-162 (In Korean).

Kim, S. P., J. G. Lee, M. W. Kim and S. J. Bae. 2017. Design and Application of Subsurface Darin Systems for Multipurpose Farmland. The 2017 KSAE Annual Conference 15-17 October 2017. p. 187 (In Korean).

Korean Industrial Standards. KS F 2302, 2012. Test method for particle size distribution of soils.

Korean Industrial Standards. KS F 2322, 2015. Test methods for permeability of saturated soils.

Korean Industrial Standards. KS F 2502, 2014. Standard test method for sieve analysis of fine and coarse aggregates.

Lee, S. B., J. G. Jeon and J. H. Yun. 2006. Study on culvert system for improvement of drainage capacity in converted upland field from paddy. Korea Society for Agricultural Machinery 11(2):217-220 (in Korean).

Skaggs, R. W., S. Hardjoamidjojo, E. H. Wiser and E. A. Hiler. 1982. Simulation of crop response and subsurface drainage systems. Transactions of the ASAE 25(6): 1673-1678.